ACS APPLIED MATERIALS & INTERFACES

Research Article

www.acsami.org

Enhancing Charge Transfer Kinetics by Nanoscale Catalytic Cermet Interlayer

Jihwan An,[†] Young-Beom Kim,*[,†,‡] Turgut M. Gür,[§] and Fritz B. Prinz[†,§]

[†]Department of Mechanical Engineering and [§]Department of Materials Science and Engineering, Stanford University, Stanford, California 94305, United States

[‡]Department of Mechanical Engineering, Hanyang University, Seoul 133-791, Korea

ABSTRACT: Enhancing the density of catalytic sites is crucial for improving the performance of energy conversion devices. This work demonstrates the kinetic role of 2 nm thin YSZ/Pt cermet layers on enhancing the oxygen reduction kinetics for low temperature solid oxide fuel cells. Cermet layers were deposited between the porous Pt cathode and the dense YSZ electrolyte wafer using atomic layer deposition (ALD). Not only the catalytic role of the cermet layer itself but the mixing effect in the cermet was explored. For cells with unmixed and fully mixed cermet interlayers, the maximum power density was enhanced by a factor of 1.5 and 1.8 at 400 °C, and by 2.3 and 2.7 at 450 °C, respectively, when compared to control cells with no cermet interlayer. The observed enhancement in cell performance is believed to be due to the increased triple phase boundary (TPB) density in the cermet interlayer. We also believe that the sustained kinetics for the fully mixed cermet layer sample stems from better thermal stability of Pt islands separated by the ALD YSZ matrix, which helped to maintain the high-density TPBs even at elevated temperature.

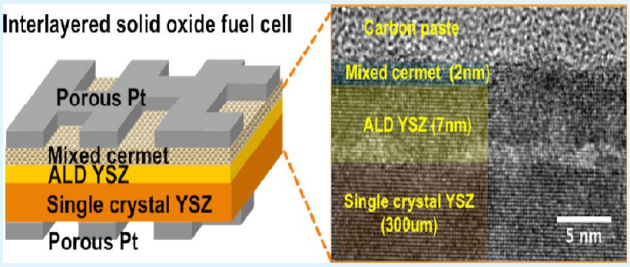

KEYWORDS: *solid oxide fuel cell, atomic layer deposition, interlayer, cermet, nanoparticle*

INTRODUCTION

There is great interest in solid oxide fuel cells (SOFCs) as sustainable energy conversion devices because of their high conversion efficiency and fuel flexibility. They usually operate at the high-temperature regime of 700−1000 °C due to relatively low ionic conductivity of solid oxide electrolytes, which poses practical problems such as thermal stress or rapid material degradation.[1] Therefore, extensive research has been done to lower the operating temperature by fabricating cell that employ thin film materials and architecture.[5,17] However, lowering the operating temperature significantly increases activation losses, especially at the cathode side because of the sluggish kinetics of the oxygen reduction reaction (ORR).[2−4]

There have been efforts to reduce the activation loss at the cathode side for low-temperature SOFC (LT-SOFC).[5−8,15,16] One of those include the use of an catalytic interlayer such as doped ceria, e.g., gadolinia-doped ceria (GDC) or yttria-doped ceria (YDC), between the electrode and the yttria-stabilized zirconia (YSZ) electrolyte.[5−8] These interlayers were shown to reduce cathodic activation loss because they have better catalytic activity and enhanced kinetics for ORR because of the significantly lower activation energy (0.07 eV for Pt/YDC) compared to doped zirconia (0.38 eV for Pt/YSZ).[7]

An alternative approach involves increasing the density of the triple phase boundary (TPB), where the electrode, the electrolyte and the gas meet. Microscale porous Pt electrode fabrication by dc magnetron sputtering has been an easy and common way to fabricate high TPB density, and e-beam or nanosphere lithography have also produced well-defined catalyst structure on the scale of a few hundred nanometers to a few micrometers.[5,9] Moreover, the possibility of using metal/ion-conducting oxide composites as electrodes has been explored to utilize the mixed electronic-ionic conduction. Ni-YSZ cermet anode is one of the most widely used anode materials for SOFCs.[10,11] For cathode materials, various kinds of cermet materials have been studied, e.g., Ag-YSZ,[12] Ag-perovskite,[13] and Pt-YSZ.[14] They are mostly fabricated by cosintering or cosputtering, which have limitations in assuring homogeneous intermixing of the deposited materials.

Atomic layer deposition (ALD) is an ideal technique for depositing thin film interlayers because it can easily deposit not only conformal films but films with varying stoichiometry by controlling the pulse ratio of individual components. For example, optimized doping of ALD YSZ[15] and YDC[16] interlayers showed an enhancement in the measured power density by a factor of 1.5 and 3.5, respectively, compared to that of the reference fuel cell membrane-electrode-assembly (MEA). Furthermore, a mixture of different phase materials, e.g., metal and oxide, can be easily fabricated using ALD by alternating the individual ALD processes for each material.

In this paper, we present the effect of ALD deposited ultrathin (<2 nm) YSZ/Pt cermet layers on kinetic activity at

Received: September 13, 2012
Accepted: November 14, 2012
Published: November 14, 2012

   dx.doi.org/10.1021/am3019788 | ACS Appl. Mater. Interfaces 2012, 4, 6790−6795

the cathode and on the overall fuel cell performance measured between 350 and 450 °C. Even though the Pt content on the interlayer surface was small, i.e., less than 2%, the introduction of the ALD YSZ/Pt cermet layer between the YSZ electrolyte and the porous Pt catalytic cathode enhanced the exchange current density up to by a factor of 2 and 3 and the maximum power density by a factor of 2.3 and 2.7 at 450 °C for nonmixed and fully mixed cermet layers, respectively. We also show that the fully mixed cermet layer produces dispersed Pt nanoparticles with smaller sizes and higher density than the nonmixed cermet layer even after annealing, which helps to form high density TPB at the electrode/electrolyte interface.

EXPERIMENTAL SECTION

The precursors used for ALD fabrication of YSZ were tetrakis-(dimethylamido) zirconium ($Zr(NMe_2)_4$) (Sigma Aldrich) for depositing zirconia and tris-(methylcyclopentadienyl) yttrium ($Y(MeCp)_3$) (Strem Chemical) for yttria. Water was used as the oxidant for both precursors. Six zirconia deposition cycles and one yttria cycle constitute one super cycle, whose growth rate is ~7 Å/supercycle and the resulting composition is determined to be 8 mol % yttria doped zirconia.[17] For ALD of Pt, trimethyl(methylcyclopentadienyl) platinum(IV) (99%, Strem Chemicals) was used as the precursor and air as the oxidant. The growth rate for Pt was 0.5−0.6 Å/cycle.[18,26] The substrate temperature was maintained at 250 °C for both of YSZ and Pt deposition. We fabricated three different MEA samples, namely, the reference, nonmixed, and fully mixed cermet interlayer structures. For all of them, we used single crystalline YSZ substrates (Marketek, 1 cm × 1 cm, 300 μm thick) containing 8 mol % of yttria doping. Then 7 nm of ALD YSZ was deposited on top of the substrates to ensure similar surface roughness for the samples. One of these samples was employed as the "reference" MEA. Subsequently, 14 cycles of ALD YSZ followed by 14 cycles of ALD Pt were deposited on top of sample 2 to fabricate the nonmixed cermet sample. For making the fully mixed cermet, we mixed the same number of ALD YSZ and Pt cycles, i.e., (one zirconia or yttria layer and one Pt layer) × 14 cycles, on top of sample 3 as the functional interlayer. The functional layer was not deposited on sample 1, which served as the reference sample (Figure 1d, e). After this operation, conventional porous Pt layer of 80 nm was deposited on both sides of the all samples using dc sputtering under 50 W of plasma power at an Ar pressure of 10 Pa at room temperature (Figure 1).

For fuel cell performance measurements, a customized test station developed in our laboratory was used as described in the earlier publication.[5] Pure hydrogen was used as fuel on the anode side, and the cathode side was exposed to ambient air. The temperature was controlled by an embedded heater placed under the chamber. Measurements were done at 350, 400, and 450 °C. A Gamry Potentiostat (FAS2, Gamry Instruments, Inc.) unit was used for the acquisition of current−voltage data, and electrochemical impedance spectroscopy (EIS) was used in the frequency range of 300 kHz to 0.1 Hz with an a.c. signal amplitude of 100 mV. EIS results were analyzed by Z-plot software based on the complex nonlinear least-squares fitting method.

For the compositional analysis of the sample surface, we used XPS (PHI VersaProbe Scanning XPS Microprobe) with Al (Kα) radiation (1486 eV). To minimize the sampling depth, we used angle-resolved XPS (ARXPS) technique with a takeoff angle of 15 ^{0}, whose analyzing depth is approximately 2−3 nm. The surface survey scan was run from a binding energy of 0 eV up to 800 eV with a step size of 0.5 eV. The high-resolution scan was run with a step size of 0.05 eV.

For morphological characterization, transmission electron microscopy (TEM, FEI Tecnai G2 F20 X-TWIN) was utilized. ALD Pt and ALD Pt/YSZ cermet layers were deposited on TEM grid with 8 nm freestanding amorphous SiO_2 membrane (Ted Pella, Inc.). For surface topography analysis, we used AFM (Park Systems XE-70 model) with the scanning window size of 500 nm × 500 nm in noncontact mode.

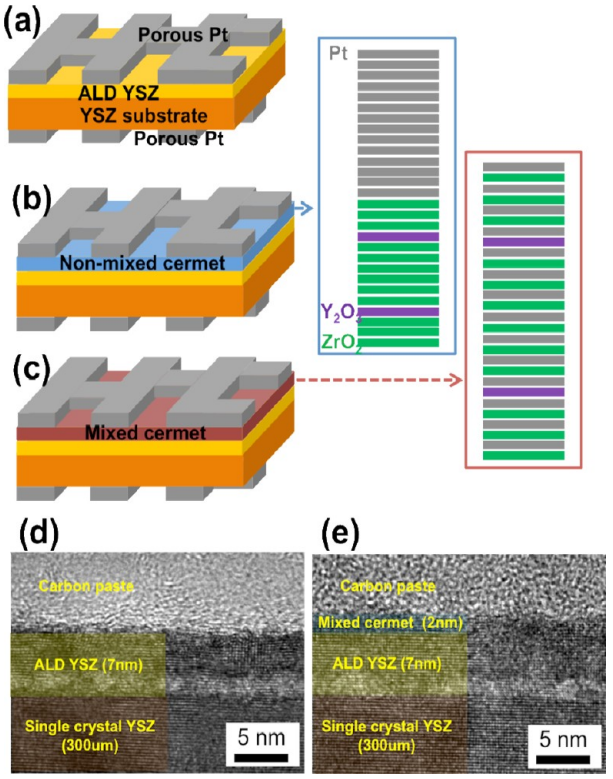

Figure 1. Schematic of sample structures: (a) reference (without cermet interlayer), (b) nonmixed cermet interlayer, and (c) mixed cermet interlayer samples. TEM cross-sectional images of the (d) nonmixed cermet interlayer and (e) mixed cermet interlayer.

The root-mean-square (RMS) roughness was analyzed by XEI software.

RESULTS AND DISCUSSION

Fuel cell current−voltage (i.e., $I-V$) performance and power densities of the MEAs were measured at 350, 400, and 450 °C using pure hydrogen fuel at 20 sccm on the anode and air on the cathode as shown in Figure 2. Open circuit voltages (OCVs) ranged between 1.04 and 1.10 V at 450 °C, between 1.01 and 1.07 V at 400 °C and between 1.02 and 1.05 V at 350 °C. OCV values were less than the theoretical value by the Nernst equation (1.20 V at 450 °C).[19] This is possibly due to a slight leak of hydrogen through the gold ring seal. Even though the power density enhancement was not significant at 350 °C, the introduction of the nonmixed and fully mixed ALD YSZ/Pt cermet interlayer increased the maximum power density by a factor of 1.5 and 1.8 at 400 °C, and 2.3 and 2.7 at 450 °C (Figure 2). The maximum power densities at these temperatures are summarized in Figure 3.

As shown in Figure 2, no significant voltage drop is observed near the low voltage region. As expected with the 300 mm thick YSZ electrolyte, ohmic losses seem to dominate the $I-V$ behavior. The activation loss, in which the cathodic contribution is dominant,[2−4] can be expressed as follows[8]

$$\eta_{act} = \mathrm{OCV} - V_{meas} - j\mathrm{ASR}_e \quad (1)$$

In eq 1, OCV is the open circuit voltage, V_{meas} is the measured voltage, j is the current density, and ASR_e is the area specific resistance of the electrolyte. When j is larger than j_o, the η_{act} yields

dx.doi.org/10.1021/am3019788 | ACS Appl. Mater. Interfaces 2012, 4, 6790−6795

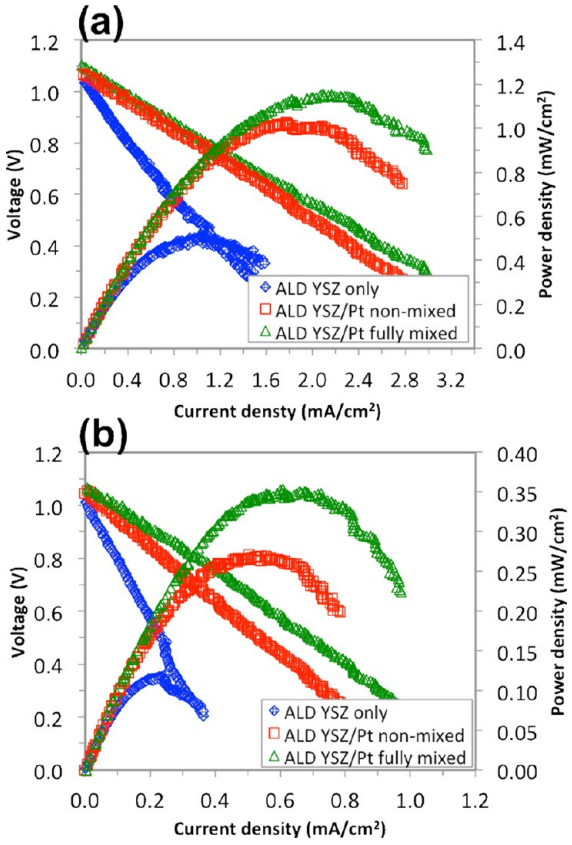

Figure 2. Current–voltage and power density curves of samples at (a) 450 °C and (b) 400 °C.

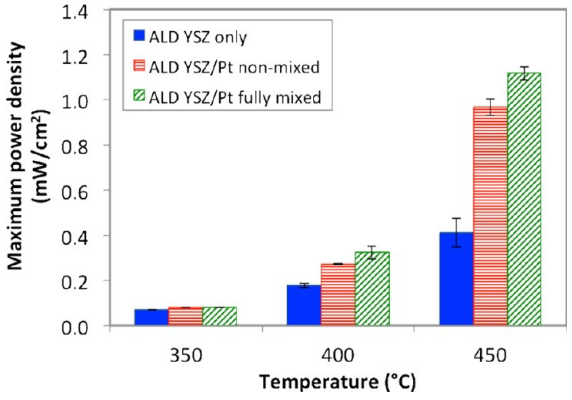

Figure 3. Maximum power densities of the samples according to the measuring temperature.

$$\eta_{act} = -\frac{RT}{\alpha nF}\ln j_0 + \frac{RT}{\alpha nF}\ln j \qquad (2)$$

The Tafel plot of the activation loss vs ln(j), when fitted to a straight line in the high overvoltage region, provides the exchange current density j_0 obtained from the y-axis intercept.[19] The Tafel plots with representing fitting lines are shown in Figure 4. The calculated j_0 values were 0.064, 0.128, and 0.188 mA/cm^2 with fitting errors of 3.4, 3.7, and 1.6% for the reference, nonmixed, and fully mixed samples, respectively. These results indicate that the power density enhancement in MEAs with ALD YSZ/Pt layers are likely due to the enhanced rates at the cathodes.

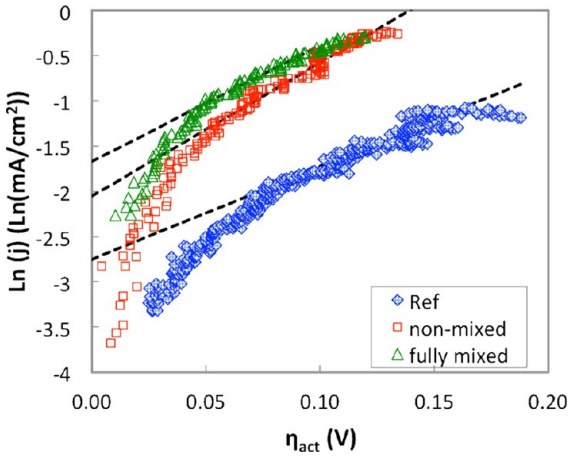

Figure 4. Tafel plot of the three samples.

For further investigation of the sources of the observed losses, we performed EIS analysis between the frequency range of 300kHz and 0.1 Hz (Figure 5). The EIS spectra consisted of 2 semicircles: One is due to the electrolyte impedance in the high frequency range and is independent of the cell voltage. The other is due to the electrode impedance at the low frequency range and is affected by cell voltage as shown in Figure 5a. The electrode impedance is mainly from the cathode side in LT-SOFC. As shown in b and c in Figure 5, the electrode resistance is the biggest in the reference sample (sample 1), becomes smaller in the nonmixed cermet sample (sample 2), and shows the minimum in the fully mixed cermet sample (sample 3). This implies that oxygen reduction rates at the cathode are enhanced in samples with cermet interlayers, and the enhancement was most significant in the fully mixed sample.

These results support the conclusion that the higher power density of MEAs with ALD YSZ/Pt cermet layers is due to enhanced oxide ion kinetics at the cathode side. To provide further microscopic evidence about this enhancement, we employed ARXPS to investigate the chemical composition and the valence states of the elements near the surface (<3 nm). Figure 6 shows the XPS spectra of the MEA surfaces. In the survey scan shown in the bigger window, Zr, Y and Pt peaks are clearly visible. Quantification of elemental composition showed that the Pt content was 0, 1.6 and 1.8% at the surface and the Pt-to-Zr ratio was 0, 7.1 ± 0.03 and 7.3 ± 0.25% for the reference, nonmixed, and fully mixed samples, respectively. The significant difference between Zr and Pt ratio can be explained by the previous reports which studied the different growth rate of ALD in mixed material compared to binary oxides.[20,21] This shows that the impregnation of the YSZ surface layer with only a very small amount of Pt led to a large improvement in power density. Also it implies that the enhanced oxide ion kinetics in the fully mixed sample, compared to that in the nonmixed one, is not merely the result of the difference in Pt content. Moreover, the HRXPS spectrum in the vicinity of Pt 4f5 (74 eV) and 4f7 (71 eV) shows that Pt 4f5 and 4f7peaks for nonmixed and fully mixed samples are 73.8, 70.7 eV and 74.1, 70.9 eV, respectively. This suggests that the Pt in both samples exists as elemental Pt, and is not involved in the formation of second phase compounds such as PtZr, etc.[22]

To investigate the surface morphology in microscopic scale, we took TEM images of samples as shown in Figure 7. Both in ALD Pt only and fully mixed cermet samples, Pt islands are

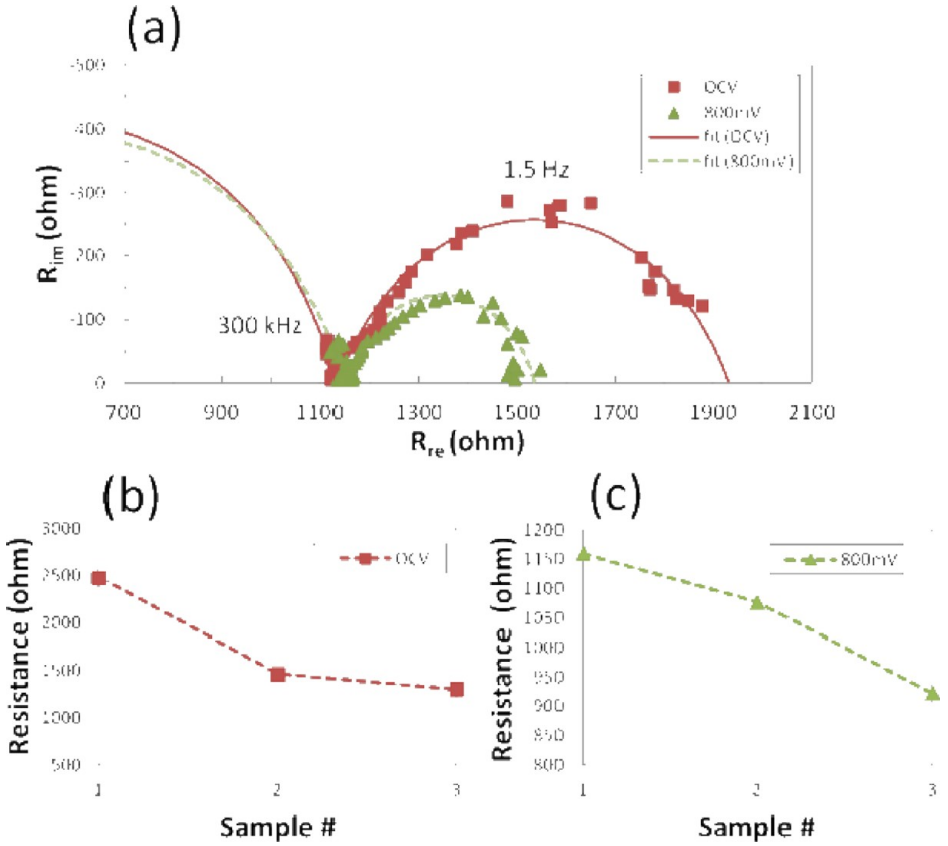

Figure 5. (a) Example of EIS spectra of the sample with fully mixed cermet layer at 450 °C at OCV and 0.8 V cell voltages. Similarly, electrode resistances of the samples at 400 °C are provided at (b) OCV and (c) 0.8 V. Samples 1, 2, and 3 denote the reference, nonmixed, and fully mixed MEAs, respectively.

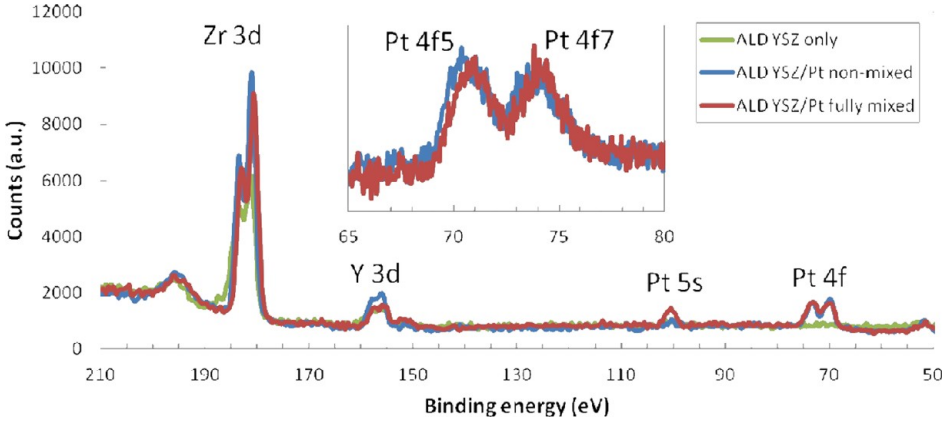

Figure 6. XPS spectra of the three MEA samples. Inset image is the HRXPS spectrum near Pt 4f peaks.

clearly visible in darker contrast because of stronger scattering of the electrons.. It is notable that there are still Pt islands in the fully mixed sample even though we alternated YSZ cycles and Pt cycles, one after another. After annealing at 450 °C for 30 min, the Pt islands in ALD Pt only samples undergo severe morphological changes, e.g., the deviation in particle sizes increases by 2-fold, the average number of particles decreases by 14% and the resulting TPB density decreases by 30%. This phenomenon, which also has been reported in previous papers,[23,24] may be due to surface diffusion of Pt islands or Oswald ripening. By contrast, the morphology of Pt particles in the fully mixed cermet layer changes only slightly upon annealing, thus preserving the TPB density (Table 1). Expectedly, the ALD YSZ matrix filling in the spaces among the Pt particles (Figure 7d, red inset) inhibit surface diffusion of Pt islands so that the coarsening effect is significantly reduced. In fact, surface morphology of the substrate is known to affect the movement of the surface atoms,[24] but further investigation is necessary to fully understand this phenomenon.

Surface morphologies of the nonmixed and fully mixed Pt particles indicate different coarsening effects. This is shown in AFM images of Figure 8, which are taken from the actual samples after fuel cell operation. The RMS value of surface roughness for the reference sample was 4.20 ± 0.45 Å, which implies that the nanogranular surface of ALD YSZ is quite smooth. The RMS roughness of the nonmixed cermet layer was

dx.doi.org/10.1021/am3019788 | ACS Appl. Mater. Interfaces 2012, 4, 6790−6795

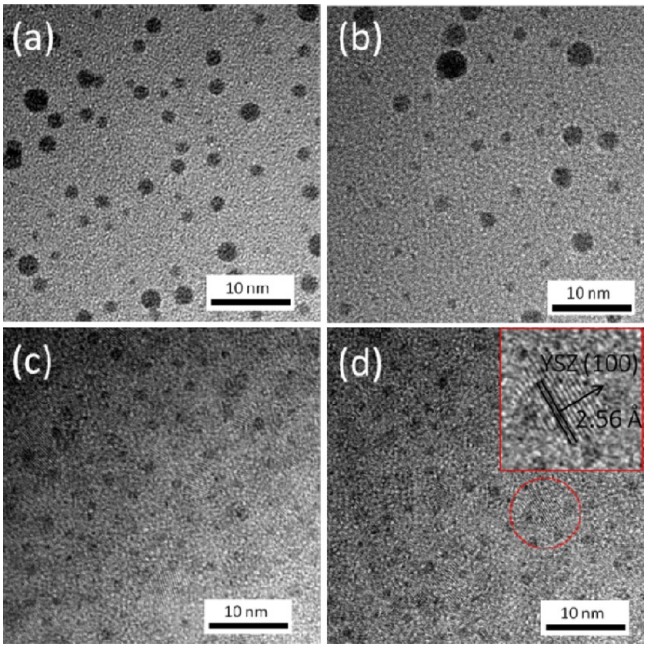

Figure 7. Bright-field TEM images of (a) as-deposited and (b) annealed samples of 14 cycles of ALD Pt only, and (c) as-deposited and (d) annealed samples of ALD YSZ/Pt fully mixed cermet. The inset in d is the zoomed-in image of the red-dotted circle area, which is the YSZ matrix. The lattice parameter measured in ALD YSZ matrix (5.12 Å) matches well to the reported value.[o].

Table 1. Statistics of Pt Islands in TEM Images

		avg diameter (nm)	avg number (in 40 × 40 nm^2)	TPB density (nm/nm^2)
nonmixed	as-deposited	1.62 ± 0.07	50.7	0.153
	annealed	1.50 ± 0.15	43.3	0.104
fully mixed	as-deposited	1.13 ± 0.05	83	0.175
	annealed	1.11 ± 0.04	80.3	0.169

significantly larger as 14.28 ± 1.06 Å due to the Pt particle coarsening effect upon annealing. The coarsened, and therefore grown-in-size Pt particles are shown in bright contrast in the image. On the contrary, the RMS roughness of the fully mixed cermet layer was 4.58 ± 0.36 Å, which is quite comparable to that of the reference sample.

On the basis of these results, we think that Pt particles in the fully mixed cermet layer were not fully covered by overlaying YSZ layer, but still in contact with the gas, i.e, air in this case, preserving the density of TPBs. Notably, enhanced cathode kinetics was observed in samples with cermet interlayers even when Pt particles are not connected to each other and to the current collector, i.e., when percolation among Pt particles is lacking. Even though the exact mechanistic model of oxygen reduction at Pt/YSZ interface has not been fully developed and agreed,[27] we speculate that the adsorbed oxygen on the surface of gas-exposed Pt particles diffuse to the Pt particle/YSZ interface, and further to the interface between porous Pt/YSZ interface along the YSZ surface. The oxygen is then reduced along the porous Pt/YSZ interface by accepting electrons and incorporates into the electrolyte. We believe that further investigation of the individual process steps of the incorporation reaction is necessary to elucidate the mechanistic details of its elementary steps more thoroughly.

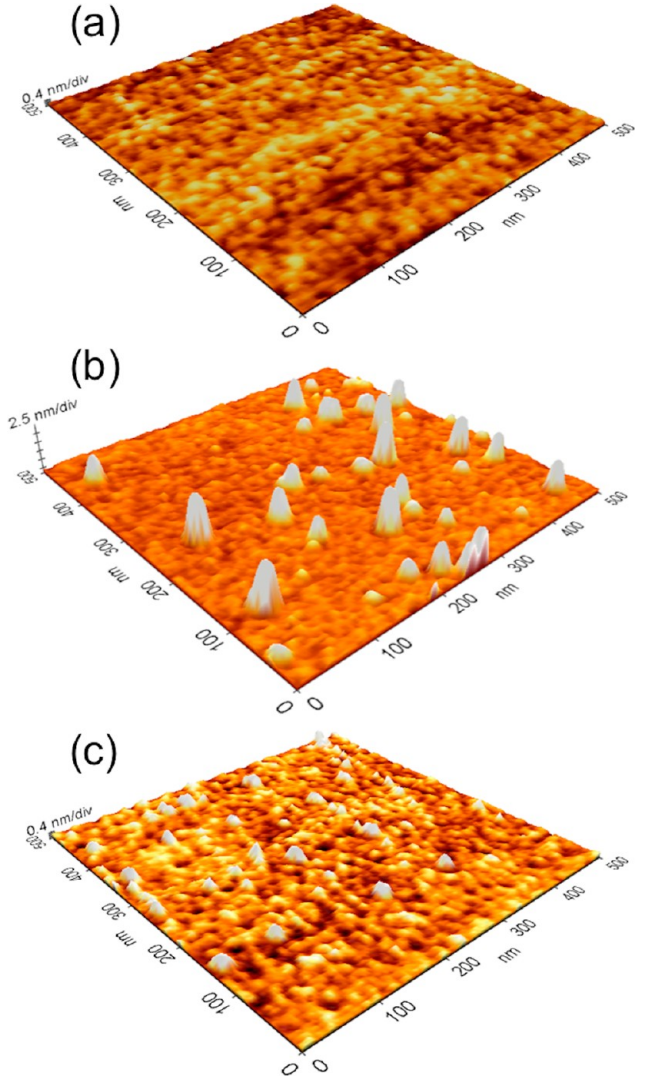

Figure 8. AFM surface images of the MEA samples ((a) reference, (b) non-mixed, and (c) fully mixed cermet layers) after fuel cell operation. All images were taken in 500 nm × 500 nm windows. Z-scales are identical.

CONCLUSION

MEAs with ultrathin ALD YSZ/Pt cermet interlayers were fabricated and tested for their fuel cell performances. The MEA with a fully mixed cermet layer showed higher power densities than the reference MEA or the MEA with a nonmixed cermet layer. The analysis by Tafel plot and EIS implied that this improvement stems from the enhancement in the surface exchange current, and the decrease in the activation loss is due to the enhanced rate at the cathode. Moreover, TEM and AFM results suggested that the fully mixed cermet provides thermal stability of the Pt particles, which preserved the TPB density at elevated operating temperature. We expect that these thermally stable cermet layers can potentially be used not only for fuel cell applications but also for other energy conversion devices that need large density of catalytically active sites, such as electrolyzers, catalytic converters for emission gas, etc.

AUTHOR INFORMATION

Corresponding Author

*E-mail: ybkim@hanyang.ac.kr.

Author Contributions

The manuscript was written through contributions of all authors.

Notes

The authors declare no competing financial interest.

■ ACKNOWLEDGMENTS

J.A. gratefully acknowledges the financial support from Kwanjeong Educational Foundation. Y.-B.K. acknowledges financial supports from Korea National Research Foundation (contract no. 2012R1A1A1014689). The authors also thank Prof. Joop Schoonmann for valuable discussions. J.A.,T.M.G., and F.B.P. gratefully acknowledge partial support from the Center on Nanostructuring for Efficient Energy Conversion (CNEEC) at Stanford University, an Energy Frontier Research Center funded by the U.S. Department of Energy, Office of Science, Office of Basic Energy Sciences under Award Number DE-SC0001060.

■ REFERENCES

(1) Steele, B. C. H.; Heinzel, A. *Nature* **2001**, *414*, 345.
(2) Horita, T.; Yamaji, K.; Sakai, N.; Xiong, Y.; Kato, T.; Yokokawa, H.; Kawada, T. *J. Power Sources* **2002**, *106*, 224.
(3) Sasaki, K.; Tamura, J.; Hosoda, H.; Lan, T.; Yasumoto, K.; Dokiya, M. *Solid State Ionics* **2002**, *148*, 551.
(4) Xia, C.; Rauch, W.; Chen, F.; Liu, M. *Solid State Ionics* **2002**, *149*, 11.
(5) Huang, H.; Nakamura, M.; Su, P.; Fasching, R.; Saito, Y.; Prinz, F. B. *J. Electrochem. Soc.* **2007**, *154*, B20.
(6) Kim, Y. B.; Shim, J. H.; Gür, T. M.; Prinz, F. B. *J. Electrochem. Soc.* **2011**, *158*, 1453.
(7) Kim, Y. B.; Holme, T. P.; Gür, T. M.; Prinz, F. B. *Adv. Funct. Mater* **2011**, *21*, 1.
(8) Fan, Z.; Prinz, F. B. *Nano Lett.* **2011**, *11*, 2202.
(9) Kim, Y. B.; Hsu, C. -M.; Connor, S. T.; Gür, T. M.; Cui, Y.; Prinz, F. B. *J. Electrochem. Soc.* **2010**, *157*, B1269.
(10) Jiang, S. P.; Chan, S. H. *J. Mater. Sci.* **2004**, *39*, 4405.
(11) Kim, J. W.; Virkar, A. V.; Fung, K. Z.; Mehta, K.; Singhal, S. C. *J. Electrochem. Soc.* **1999**, *146*, 69.
(12) Wang, L. S.; Thiele, E. S.; Bartnett, S. A. *Solid State Ionics* **1992**, *52*, 261.
(13) Wang, L. S.; Barnett, S. A. *Solid State Ionics* **1995**, *76*, 103.
(14) Hertz, J. L.; Tuller, H. L. *J. Electrochem. Soc.* **2007**, *154*, B413.
(15) Chao, C. -C.; Kim, Y. B.; Prinz, F. B. *Nano Lett.* **2009**, *9*, 3626.
(16) Fan, Z.; Chao, C. -C.; Hossein-Babaei, F.; Prinz, F. B. *J. Mater. Chem.* **2011**, *21*, 10903.
(17) Shim, J.; Chao, C. -C.; Huang, H.; Prinz, F. B. *Chem. Mater.* **2007**, *19*, 3850.
(18) Aaltonen, T.; Ritala, M.; Sajavaara, T.; Keinonen, J.; Leskela, M. *Chem. Mater.* **2003**, *15*, 1924.
(19) O'Hayre, R.; Cha, S.; Colella, W.; Prinz, F. B. *Fuel Cell Fundamentals*; John Wiley and Sons: New York, 2006.
(20) Vehkamaki, M.; Hatanpaa, T.; Hanninen, T.; Ritala, M.; Leskela, M. *Electrochem. Solid-State Lett.* **1999**, *2*, 504.
(21) Putkonen, M.; Sajavaara, T.; Niinisto, J.; Johansson, L. S.; Niinisto, L. *J. Mater. Chem.* **2002**, *12*, 442.
(22) Moulder, J. F.; Stickle, W. F.; Sobol, P. E.; Bomben, K. D., *Handbook of X-ray Photoelctron Spectroscopy*; ULVAC-PHI, Inc.: Chigasaki, Japan, 1995.
(23) Wen, J. −M.; Evans, J. W.; Bartelt, M. C.; Burnett, J. W.; Thiel, P. A. *PRL* **1966**, *76*, 652.
(24) Pai, W. W.; Swan, A. K.; Zhang, Z.; Wendelken, J. F. *PRL* **1997**, *79*, 3210.
(25) Pomfret, M. B.; Stoltz, C.; Varughese, B.; Walker, R. A. *Anal. Chem.* **2005**, *77*, 1791.
(26) Jiang, X.; Bent, S. F. *J. Electrochem. Soc.* **2007**, *154*, D648.
(27) Adler, S. B. *Chem. Rev.* **2004**, *104*, 4791−4843.